Matrix Isolation Infrared Spectroscopic and Theoretical Study of Transition Metal Dioxide−Acetylene Complexes

Mingfei Zhou,* Jian Dong, and Lei Miao

Shanghai Key Laboratory of Molecular Catalysts and Innovative Materials, Department of Chemistry & Laser Chemistry Institute, Fudan University, Shanghai 200433, People's Republic of China

Received: December 14, 2003; In Final Form: February 3, 2004

The reactions of transition metal dioxides (MnO_2 and FeO_2) with acetylene molecules have been studied using matrix isolation infrared absorption spectroscopy. The metal dioxide molecules were prepared by the reactions of laser-ablated metal atoms with dioxygen. In solid argon, the MnO_2 and FeO_2 molecules reacted with C_2H_2 to form the (η^2-C_2H_2)MnO_2 and (η^2-C_2H_2)FeO_2 complexes spontaneously on annealing. Both complexes were predicted to have low-spin ground states ($^1A_1$ for (η^2-C_2H_2)FeO_2, $^2A_1$ for (η^2-C_2H_2)MnO_2) with C_{2v} symmetry. In addition, evidence is also presented for the formation of Mn(H)CCO and Fe(H)CCO molecules upon UV−visible irradiation. The product absorptions were identified by isotopic substitution as well as density functional calculations of isotopic frequencies.

Introduction

Transition metal oxides, such as manganese and iron oxides, are widely used as catalysts or catalytic supports in many industrially important redox-based reactions. For example, manganese dioxide is used to oxidize allylic and benzylic alcohols to the corresponding carbonyl compounds, to dehydrogenate cyclic compounds to arenes, and to catalyze the C−C bond cleavage of glycols.[1] High-valent iron−oxo species are proposed to be the key reactive species that effect substrate oxidation in many heme and nonheme iron enzymes.[2−5] In cytochrome P450, the iron(IV)−oxo moiety is used in conjunction with a porphyrin radical to effect hydroxylations of alkanes and arenas. In methane monooxygenase (MMO), two iron(IV)−oxo species work in concert to achieve oxidation of methane to methanol. Previous studies have provided a wealth of insight concerning the reactivity of bare manganese and iron metal atoms, cations as well as oxide cations with hydrocarbons such as small alkanes and alkenes.[6−16] By contrast, the reactions of neutral manganese and iron oxide molecules with small hydrocarbons are relatively less studied.

Recent investigations in our laboratory have shown that laser ablation combined with matrix isolation is a suitable technique in producing metal dioxide molecules for reaction study.[17−23] As has been mentioned, the primary products from co-deposition of some laser-ablated metal atoms with oxygen in excess argon are predominantly metal dioxide molecules. Hence, reactions of the primary formed metal dioxide molecules with other small molecules doped in the reagent gas have been reported.[17−21] For instance, the titanium dioxide molecule reacted with acetylene to form a stable TiO_2–C_2H_2 complex in solid argon. The complex underwent photochemical rearrangement to the OTi(OH)CCH and $H_2Ti(CO)_2$ isomers.[17] Here we report similar studies on the reactions of manganese and iron dioxides (FeO_2 and MnO_2) with acetylene molecules. These acetylene and transition metal dioxide reactions may serve as a simple model for understanding the interactions of transition metal oxides with other more complicated organic substrates.

* Corresponding author. E-mail: mfzhou@fudan.edu.cn.

Experimental and Computational Methods

The experimental setup for pulsed laser ablation and matrix isolation FTIR spectroscopic investigation has been described in detail previously.[24] Briefly, the 1064 nm fundamental of a Nd:YAG laser (20 Hz repetition rate and 8 ns pulse width) was focused onto a rotating manganese or iron metal target through a hole in a CsI window. The laser-ablated metal atoms were co-deposited with oxygen and acetylene mixtures in excess argon onto the 12 K CsI window for 1 h at a rate of 3−5 mmol/h. C_2H_2 was subjected to several freeze−pump−thaw cycles before use. O_2 (Shanghai BOC, 99.6%), $^{13}C_2H_2$ and C_2D_2 (99%, Cambridge Isotope Laboratories), and $^{18}O_2$ (Isotec Inc., >97%) were used without further purification. Infrared spectra were recorded on a Bruker IFS 113V spectrometer at 0.5 cm^{-1} resolution using a DTGS detector. Matrix samples were annealed at different temperatures, and selected samples were subjected to broad-band irradiation using a high-pressure mercury arc lamp.

Density functional theoretical (DFT) calculations were performed using the Gaussian 98 program.[25] The Becke three-parameter hybrid functional with the Lee−Yang−Parr correlation corrections (B3LYP) was used.[26,27] The 6-311++G** basis set was used for H, C, and O atoms. The all-electron basis set of Wachters−Hay as modified by Gaussian was used for Fe and Mn atoms.[28,29] Geometries were fully optimized and vibrational frequencies calculated with analytical second derivatives, and zero point vibrational energies were derived.

Results and Discussion

Matrix-isolated iron and manganese dioxide molecules were prepared by reactions of laser-ablated metal atoms with molecular oxygen in excess argon. Co-condensation of laser-ablated iron or manganese atoms with 0.8% O_2 in argon revealed strong metal dioxide (FeO_2, 945.8 and 797.0 cm^{-1}; MnO_2, 948.0 and 816.4 cm^{-1}) and O_4^- (953.8 cm^{-1}) absorptions with very weak O_3 (1039.8 cm^{-1}) and metal monoxide absorptions (FeO, 872.8 cm^{-1}; MnO, 833.3 cm^{-1}).[22,23] Subsequent 20 min broad-band irradiation with a high-pressure mercury lamp destroyed the O_4^-

10.1021/jp0378586 CCC: $27.50
Published on Web 03/05/2004

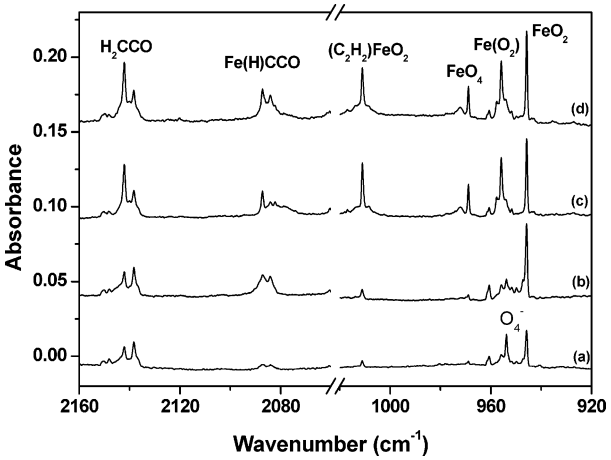

Figure 1. Infrared spectra in the 2160−2060 and 1020−920 cm^{-1} regions from co-deposition of laser-ablated iron atoms with 0.3% C_2H_2 + 0.8% O_2 in argon: (a) 1 h sample deposition at 12 K, (b) 20 min broad-band irradiation, (c) 25 K annealing, and (d) 20 min broad-band irradiation.

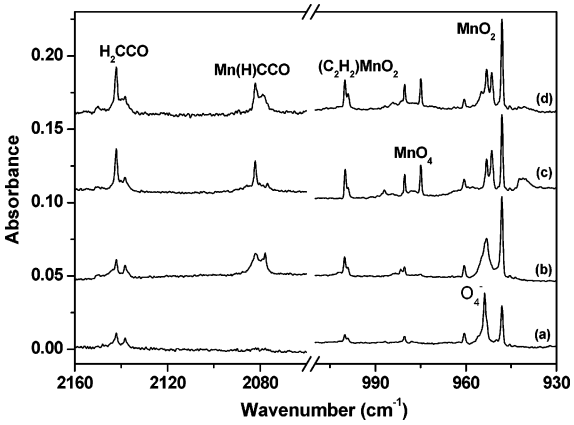

Figure 2. Infrared spectra in the 2160−2060 and 1010−930 cm^{-1} regions from co-deposition of laser-ablated manganese atoms with 0.3% C_2H_2 + 0.8% O_2 in argon: (a) 1 h sample deposition at 12 K, (b) 20 min broad-band irradiation, (c) 25 K annealing, and (d) 20 min broad-band irradiation.

TABLE 1: Product Absorptions (cm^{-1}) from Co-deposition of Laser-Ablated Iron or Manganese Atoms with O_2/C_2H_2 Mixtures in Excess Argon (H_2CCO, FeO_2, and MnO_2 Absorptions Also Listed for Comparison)

O_2/C_2H_2	$^{18}O_2/C_2H_2$	$O_2/^{13}C_2H_2$	O_2/C_2D_2	assignment
2142.1	2115.4	2080.1	2112.6	H_2CCO
2087.2	2062.8	2025.6	2074.3	Fe(H)CCO
1011.0	973.2	1010.6	1009.6	(η^2-C_2H_2)FeO_2
945.8	911.2	945.8	945.8	FeO_2
2082.2	2058.1	2020.8	2068.5	Mn(H)CCO
1000.0	962.8	999.9	999.5	(η^2-C_2H_2)MnO_2
948.0	912.6	948.0	948.0	MnO_2

absorption and markedly increased the metal dioxide absorptions. Next 25 K annealing markedly increased the $Fe(O_2)$ (955.9 cm^{-1}) and FeO_4 (968.9 cm^{-1}) or MnO_4 (974.9 cm^{-1}) absorptions.[22,23] New product absorptions appeared in similar experiments with C_2H_2 added to the reagent gas. Figures 1 and 2 show the spectra in the selected regions from co-deposition of laser-ablated iron and manganese atoms with 0.3% C_2H_2 and 0.8% O_2 in argon, and the new product absorptions are listed in Table 1. Besides the metal oxide and oxygen cluster absorptions, very weak H_2CCO,[30] CCH,[31] and HOO[32,33] absorptions were also observed after sample deposition. A 20 min broad-band irradiation produced broad new bands at 2087.2 cm^{-1} (Fe) and 2082.2 cm^{-1} (Mn). These new absorptions sharpened on subsequent annealing to 25 K, while new absorptions appeared at 1011.0 cm^{-1} (Fe) and 1000.0 cm^{-1} (Mn), which were almost kept unchanged on another 20 min broad-band irradiation.

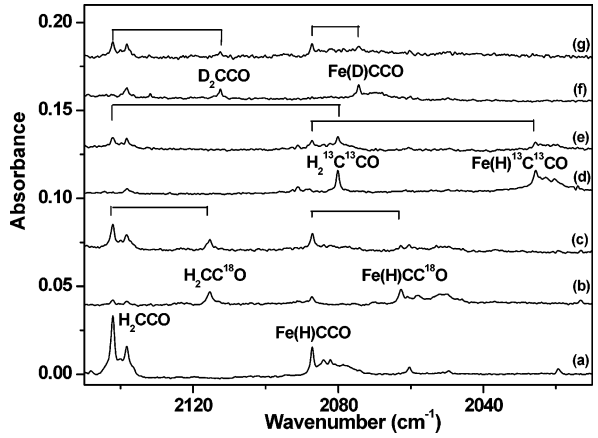

Figure 3. Infrared spectra in the 2150−2010 cm^{-1} region from co-deposition of laser-ablated iron atoms with O_2/C_2H_2 mixtures in excess argon: (a) 0.3% C_2H_2 + 0.8% O_2, (b) 0.3% C_2H_2 + 0.8% $^{18}O_2$, (c) 0.3% C_2H_2 + 1.0% ($^{16}O_2$ + $^{16}O^{18}O$ + $^{18}O_2$), (d) 0.3% $^{13}C_2H_2$ + 0.8% O_2, (e) 0.4% ($^{12}C_2H_2$ + $^{13}C_2H_2$) + 0.8% O_2, (f) 0.3% C_2D_2 + 0.8% O_2, and (g) 0.4% (C_2H_2 + C_2D_2) + 0.8% O_2.

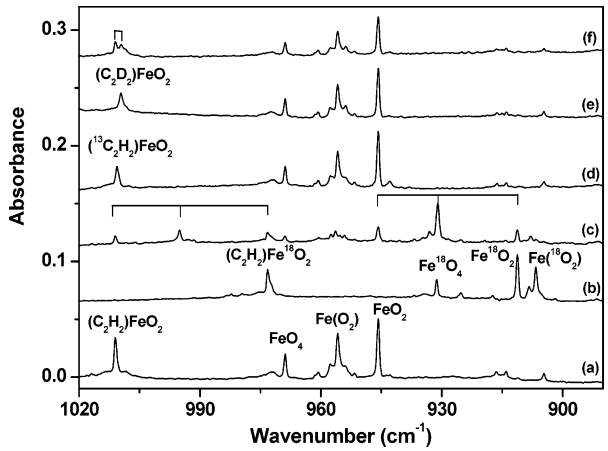

Figure 4. Infrared spectra in the 1020−890 cm^{-1} region from co-deposition of laser-ablated iron atoms with O_2/C_2H_2 mixtures in excess argon: (a) 0.3% C_2H_2 + 0.8% O_2, (b) 0.3% C_2H_2 + 0.8% $^{18}O_2$, (c) 0.3% C_2H_2 + 1.0% ($^{16}O_2$ + $^{16}O^{18}O$ + $^{18}O_2$), (d) 0.3% $^{13}C_2H_2$ + 0.8% O_2, (e) 0.3% C_2D_2 + 0.8% O_2, and (f) 0.4% (C_2H_2 + C_2D_2) + 0.8% O_2.

The experiments were repeated with the O_2/C_2D_2, $O_2/^{13}C_2H_2$, O_2/C_2H_2 + C_2D_2, $O_2/^{12}C_2H_2$ + $^{13}C_2H_2$, $^{18}O_2/C_2H_2$, and $^{16}O_2$ + $^{16}O^{18}O$ + $^{18}O_2/C_2H_2$ samples. The isotopic shifts and splittings of the new product absorptions will be discussed in detail below. Representative spectra in selected regions using different isotopic samples are shown in Figures 3 and 4, respectively.

(η^2-C_2H_2)FeO_2. The band at 1011.0 cm^{-1} in the Fe + O_2/C_2H_2 experiments exhibited very small carbon-13 (0.4 cm^{-1}) and deuterium (1.4 cm^{-1}) isotopic shifts. However, when an $^{18}O_2/C_2H_2$ sample was used, the band was observed at 973.2 cm^{-1}. The $^{16}O/^{18}O$ isotopic frequency ratio of 1.0388 indicates that this band is predominantly an antisymmetric OFeO stretching vibration. In the $^{16}O_2$ + $^{16}O^{18}O$ + $^{18}O_2/C_2H_2$ experiment, a triplet at 1011.0, 995.0, and 973.2 cm^{-1} was observed, indicating that two equivalent oxygen atoms are involved in this mode. This band is 65.2 cm^{-1} higher than the antisymmetric stretching vibration of FeO_2, so an FeO_2 complex should be considered. The small carbon-13 and deuterium isotopic shifts imply the

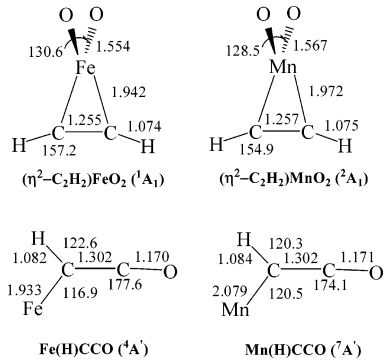

Figure 5. Optimized structures for the ground state $(\eta^2\text{-}C_2H_2)MO_2$ and M(H)CCO (M = Fe and Mn) molecules (bond lengths in angstroms, bond angles in degrees).

TABLE 2: Calculated Vibrational Frequencies (cm^{-1}) and Intensities (in Parentheses, km/mol) for $(\eta^2\text{-}C_2H_2)MO_2$ and M(H)CCO (M = Fe, Mn)

$(\eta^2\text{-}C_2H_2)FeO_2$ ($^1A_1$)	Fe(H)CCO ($^4A'$)	$(\eta^2\text{-}C_2H_2)MnO_2$ ($^2A_1$)	Mn(H)CCO ($^7A'$)
3356.9 (18, a_1)	3196.5 (22, a′)	3341.5 (19, a_1)	3190.5 (17, a′)
3290.7 (53, b_2)	2153.7 (1306, a′)	3279.1 (44, b_2)	2146.8 (1308, a′)
1780.6 (25, a_1)	1252.3 (23, a′)	1768.4 (31, a_1)	1253.6 (18, a′)
1078.3 (273, b_1)	946.0 (116, a′)	1067.9 (294, b_1)	943.3 (113, a′)
980.2 (66, a_1)	607.7 (4, a′)	1009.2 (57, a_1)	609.0 (4, a′)
822.4 (53, b_2)	585.7 (8, a″)	834.3 (60, b_2)	587.2 (6, a″)
785.7 (4, a_1)	441.4 (51, a′)	780.9 (4, a_1)	421.6 (63, a′)
763.0 (0, a_2)	393.8 (48, a″)	770.7 (0, a_2)	382.1 (51, a″)
748.6 (38, b_1)	105.4 (1, a′)	723.8 (45, b_1)	101.0 (1, a′)
563.3 (0, b_2)		567.1 (2, b_2)	
475.9 (6, a_1)		479.3 (4, a_1)	
307.7 (11, a_1)		320.4 (4, a_1)	
240.2 (5, b_1)		236.2 (0, a_2)	
206.9 (0, a_2)		232.2 (3, b_1)	
191.0 (6, b_2)		178.9 (14, b_2)	

involvement of C_2H_2 in the complex. The doublet feature in the $O_2/C_2H_2 + C_2D_2$ spectrum suggests the involvement of only one C_2H_2 unit. Therefore, we assign the 1011.0 cm^{-1} band to the antisymmetric OFeO stretching mode of the $FeO_2-C_2H_2$ complex.

To support the spectroscopic assignment of the $FeO_2-C_2H_2$ complex, we performed density functional calculations. Several spin multiplicities and geometry structures were optimized to ferret out the most stable electronic states and geometries. The lowest energy structure found is illustrated in Figure 5, and the vibrational frequencies and intensities are listed in Table 2. We have optimized singlet and triplet spin states for two C_{2v} structures (a planar structure and a nonplanar structure with the FeO_2 plane perpendicular to the FeC_2 plane). Both the lowest singlet and triplet states have the nonplanar structure with the FeC_2 plane perpendicular to the FeO_2 plane. The frequency calculations indicate that the planar structure is the only transition state with imaginary frequencies. The singlet ($^1A_1$) and triplet ($^3A_2$) spin states of the nonplanar structure are very close in energy. At the B3LYP/6-311++G** level, the singlet state ($^1A_1$) was predicted to be slightly more stable than the triplet state ($^3A_2$) by about 0.2 kcal/mol. We note that previous studies on FeO_2 indicated that the B3LYP functional did not provide good energy predictions, whereas the CCSD(T) calculations predicted the appropriate ground state.[23] To further ascertain the relative stability of the singlet and triplet states, high level ab initio calculations were performed. We carried out single point calculations with the CCSD(T)/6-311++G** method at the optimized geometries of the B3LYP/6-311++G** calculations.[34] These calculations found the singlet state lower in energy than the triplet state by about 11.6 kcal/mol. Therefore, we conclude that the ground state of $(\eta^2\text{-}C_2H_2)FeO_2$ is the $^1A_1$ singlet. DFT calculations predicted the strong antisymmetric OFeO stretching mode for the singlet ground state $(\eta^2\text{-}C_2H_2)$-FeO_2 at 1078.3 cm^{-1}, just 6.6% higher than the observed value. Table 3 summarizes the comparison of the experimental and theoretical isotopic frequency ratios. The calculated isotopic frequency ratios are in good agreement with the observed values. As listed in Table 2, the antisymmetric OFeO stretching mode was predicted to have the largest IR intensity (273 km/mol). Besides this observed mode, the antisymmetric C−H stretching, symmetric OFeO stretching, and C−H deformation modes were predicted to have appreciable intensities (53, 66, and 53 km/mol); however, we were not able to observe these bands. As has been pointed out,[35] DFT calculations do not provide very reliable IR intensity predictions in some cases. It is found that the IR intensities of vibrations such as C−H stretching are substantially overestimated by DFT calculations.[15,16,35] The C−H stretching and symmetric OFeO stretching modes also may be overlapped by the strong acetylene polymer and iron oxide absorptions in the expected frequency regions.

TABLE 3: Comparison between Observed and Calculated Isotopic Frequency Ratios for $(\eta^2\text{-}C_2H_2)MO_2$ and M(H)CCO (M = Fe, Mn)

	calculated			observed		
molecule	$^{16}O/^{18}O$	$^{12}C/^{13}C$	H/D	$^{16}O/^{18}O$	$^{12}C/^{13}C$	H/D
$(\eta^2\text{-}C_2H_2)FeO_2$	1.0389	1.0000	1.0008	1.0388	1.0004	1.0014
Fe(H)CCO	1.0123	1.0310	1.0087	1.0118	1.0304	1.0062
$(\eta^2\text{-}C_2H_2)MnO_2$	1.0390	1.0000	1.0006	1.0386	1.0001	1.0005
Mn(H)CCO	1.0123	1.0310	1.0090	1.0117	1.0304	1.0066

In transition metal−acetylene complexes, the interactions between metal and ligand C_2H_2 are dominated by the synergic donation of electrons in π HOMO of C_2H_2 to an empty σ orbital of the metal and the back-donation of the metal π electrons to the C_2H_2 π^* orbital. Similarly, $(\eta^2\text{-}C_2H_2)FeO_2$ can be regarded as being formed by the interaction of FeO_2 with C_2H_2.The closed-shell singlet ground state of $(\eta^2\text{-}C_2H_2)FeO_2$ is somewhat surprising because the neutral FeO_2 molecule exhibits a triplet ground state with $(core)(b_1)^1(a_1)^1$ electronic configuration.[23] The a_1 orbital of FeO_2 is primarily a hybrid of the Fe 4s and $3d_{z^2}$ orbitals that is directed away from the O atoms and is largely nonbonding. The b_1 orbital is a π bonding orbital of FeO_2. When a C_2H_2 ligand interacts with the FeO_2 fragment, donation from the filled C_2H_2 bonding π orbital leads to destabilization of the iron-based a_1 orbital. By contrast, the empty C_2H_2 antibonding π orbital acts as acceptor orbital of π back-donation from FeO_2, stabilizing the FeO_2 b_1 orbital. Therefore, the closed-shell electronic structure is favored for the $(\eta^2\text{-}C_2H_2)FeO_2$ complex. The donation from the filled bonding π orbital of C_2H_2 and the back-donation to the antibonding π^* orbital of C_2H_2 decrease the C−C bond order in the C_2H_2 fragment. Consistent with this notion, the calculated C−C bond length in $(\eta^2\text{-}C_2H_2)FeO_2$ is 1.255 Å, which is intermediate between a typical C−C triple bond and a C−C double bond (the C−C bond lengths of free C_2H_2 and C_2H_4 were predicted to be 1.199 and 1.329 Å, respectively, at B3LYP/6-311++G** level). The binding energy of $^1A_1$ state $(\eta^2\text{-}C_2H_2)FeO_2$ with respect to the ground-state reagents $FeO_2(^3B_1) + C_2H_2(^1\Sigma_g^+)$ was predicted to be 26.5 kcal/mol at B3LYP/6-311++G** level, after zero point energy corrections.

$(\eta^2\text{-}C_2H_2)MnO_2$. The 1000.0 cm^{-1} band exhibited very small deuterium (0.5 cm^{-1}) and carbon-13 (0.1 cm^{-1}) isotopic shifts. The $^{18}O_2$ counterpart (962.8 cm^{-1}) gave an $^{16}O/^{18}O$ ratio of

1.0386 characteristic of an antisymmetric OMnO stretching vibration. This band gave a triplet absorption at 1000.0, 984.5, and 962.8 cm^{-1} with $^{16}O_2 + {}^{16}O^{18}O + {}^{18}O_2$. This band is assigned to $(\eta^2\text{-}C_2H_2)MnO_2$ following the example of iron.

Doublet and quartet states of C_{2v} $(\eta^2\text{-}C_2H_2)MnO_2$ structures have been optimized. The ground state is a $^2A_1$ state with the MnO_2 plane perpendicular to the MnC_2 plane (Figure 5). The lowest quartet state ($^4B_1$) is 19.5 kcal/mol higher in energy than the doublet state. The antisymmetric OMnO stretching frequency for the ground state $(\eta^2\text{-}C_2H_2)MnO_2$ was predicted at 1067.9 cm^{-1}, with the calculated isotopic frequency ratios in good agreement with the observed values (Table 3).

The bonding mechanism in $(\eta^2\text{-}C_2H_2MnO_2$ is about the same as that in $(\eta^2\text{-}C_2H_2)FeO_2$. The neutral MnO_2 molecule has a $^4B_1$ ground state with a $(core)(a_1)^1(b_1)^1(a_1)^1$ electronic configuration, whereas the ground state of $(\eta^2\text{-}C_2H_2)MnO_2$ was determined to be a $^2A_1$ state. Analogous to $(\eta^2\text{-}C_2H_2)FeO_2$, donation from the filled C_2H_2 bonding π orbital to the MnO_2 fragment leads to destabilization of the HOMO (a_1) of MnO_2, while π back-donation from MnO_2 to the empty C_2H_2 antibonding π orbital stabilizes the MnO_2 b_1 orbital. As a consequence, the low spin doublet electronic structure is favored for the $(\eta^2\text{-}C_2H_2)MnO_2$ complex. The binding energy of $^2A_1$ state $(\eta^2\text{-}C_2H_2)MnO_2$ with respect to the ground-state reagents $MnO_2(^4B_1) + C_2H_2(^1\Sigma_g)$ was predicted to be 29.8 kcal/mol at the B3LYP/6-311++G** level, after zero point energy corrections.

Fe(H)CCO. The band at 2087.2 cm^{-1} in the Fe + O_2/C_2H_2 experiments appeared on broad-band irradiation. This band shifted to 2025.6 cm^{-1} with $O_2/{}^{13}C_2H_2$ and to 2062.8 cm^{-1} with $^{18}O_2/C_2H_2$, and gave an $^{16}O/^{18}O$ isotopic frequency ratio of 1.0118 and a $^{12}C/^{13}C$ ratio of 1.0304. These ratios are about the same as that of the CCO stretching mode of H_2CCO ($^{16}O/^{18}O$, 1.0126; $^{12}C/^{13}C$, 1.0298), which is observed at 2142.1 cm^{-1} in solid argon. This indicates that the 2087.2 cm^{-1} band is due to a CCO stretching vibration. In the mixed $^{16}O_2 + {}^{16}O^{18}O + {}^{18}O_2/C_2H_2$ and $O_2/{}^{12}C_2H_2 + {}^{13}C_2H_2$ experiments, only the pure isotopic counterparts were observed, indicating that only one CCO subunit is involved in the molecule. The 2087.2 cm^{-1} band shifted to 2074.3 cm^{-1} with O_2/C_2D_2 and gave a H/D isotopic frequency ratio of 1.0062. Note that the deuterium isotopic shift of ketene (H/D ratio 1.0140) is about twice as large as the shift observed here for the 2087.2 cm^{-1} band. This suggests that there is less hydrogen involvement in the 2087.2 cm^{-1} mode than that in ketene, so only one hydrogen atom is most likely involved in the new product. Accordingly, we assign the 2087.2 cm^{-1} band to the CCO stretching mode of an Fe(H)CCO molecule with one H atom of ketene being replaced by an Fe atom.

The assignment was supported by DFT calculations. Geometry optimizations were performed in quartet and sextet states. At B3LYP/6-311++G** level, the Fe(H)CCO molecule was predicted to have a $^4A'$ ground state with planar C_s symmetry, and the lowest sextet state is 7.8 kcal/mol higher in energy than the ground state. As shown in Figure 5, the CCO subunit is slightly bent with C−C and C−O bond lengths of 1.302 and 1.169 Å. The calculated frequencies at the optimized geometry of Fe(H)CCO provided excellent support for the proposed identification of this molecule. As listed in Table 2, the CCO stretching mode was calculated at 2157.5 cm^{-1}. This mode was predicted to have the largest IR intensity (1274 km/mol versus less than 68 km/mol for the other vibrational modes). As listed in Table 3, the calculated isotopic frequency ratios are in excellent agreement with the observed values.

Mn(H)CCO. A similar band at 2082.2 cm^{-1} in the Mn + O_2/C_2H_2 experiments can be assigned to CCO stretching vibration of the Mn(H)CCO molecule. This band shifted to 2058.1, 2020.8, and 2068.5 cm^{-1} in $^{18}O_2/C_2H_2$, $O_2/{}^{13}C_2H_2$, and O_2/C_2D_2 experiments and exhibited CCO stretching isotopic frequency ratios ($^{16}O/^{18}O$, 1.0117; $^{12}C/^{13}C$, 1.0304; and H/D, 1.0066) that are about the same as that of the Fe(H)CCO molecule. For the Mn(H)CCO molecule, the ground state was predicted to be a $^7A'$ state, and a $^5A'$ state is about 3.0 kcal/mol higher in energy. The optimized geometry of the ground state is shown in Figure 5. The CCO stretching frequency of the ground-state Mn(H)CCO molecule was computed at 2146.8 cm^{-1}. The calculated isotopic frequency ratios also match the observed values very well (Table 3).

Reaction Mechanisms. The major reaction during condensation of iron and manganese atoms with O_2/C_2H_2 in excess argon is the insertion reaction of the metal atoms to form the metal dioxides as reported previously.[22,23] No obvious products from the reactions between metal atoms and acetylene were observed in the experiments, which suggest that the metal atom reaction with O_2 is given preference over the reaction with acetylene. Broad-band irradiation of the as-deposited samples significantly increased the metal dioxide absorptions. Subsequent sample annealing allowed the acetylene molecules to diffuse in solid argon and react with the primary formed metal dioxide molecules, reactions 1 and 2. These secondary reactions appear to be spontaneous and were predicted to be exothermic by about 26.5 and 29.8 kcal/mol, respectively, at B3LYP/6-311++G** level.

$$FeO_2(^3B_1) + C_2H_2(^1\Sigma_g^+) \rightarrow (\eta^2\text{-}C_2H_2)FeO_2(^1A_1) \quad (1)$$

$$MnO_2(^4B_1) + C_2H_2(^1\Sigma_g^+) \rightarrow (\eta^2\text{-}C_2H_2)MnO_2(^2A_1) \quad (2)$$

In the case of titanium, the $TiO_2-C_2H_2$ complex also was formed spontaneously on annealing. The complex underwent photochemical rearrangement to the OTi(OH)CCH and $H_2Ti(CO)_2$ isomers upon UV−visible irradiation.[17] No such structural isomers were observed in the iron and manganese reactions. The $(\eta^2\text{-}C_2H_2)FeO_2$ and $(\eta^2\text{-}C_2H_2)MnO_2$ absorptions kept almost unchanged upon broad-band irradiation.

The mechanism for the formation of Fe(H)CCO and Mn(H)CCO is not well understood. These molecules were formed on broad-band irradiation, and might be produced by the reaction between metal monoxide and CCH. Weak CCH and metal monoxide absorptions were observed in the experiments. One also may expect the formation of Fe(H)CCO and Mn(H)CCO via the reactions between metal atoms and H_2CCO or HCCO. The H_2CCO absorption was observed, but the HCCO absorption was not observed in the experiments.

Conclusions

The reactions of transition metal dioxides (MnO_2 and FeO_2) with acetylene molecules have been studied using matrix isolation infrared absorption spectroscopy. The metal dioxide molecules were prepared by the reactions of laser-ablated metal atoms with dioxygen. In solid argon, the MnO_2 and FeO_2 molecules reacted with C_2H_2 to form the $(\eta^2\text{-}C_2H_2)MnO_2$ and $(\eta^2\text{-}C_2H_2)FeO_2$ complexes spontaneously on annealing. Both complexes were predicted to have low-spin ground states having C_{2v} symmetry with the MC_2 plane perpendicular to the MO_2 plane. The binding energies with respect to the ground-state reagents were predicted to be 29.8 and 26.5 kcal/mol, respectively, at B3LYP/6-311++G** level. In addition, evidence is

also presented for the formation of Mn(H)CCO and Fe(H)CCO molecules upon UV−visible irradiation. Absorptions at 2087.2 and 2082.2 cm^{-1} are assigned to the CCO stretching frequencies of the Fe(H)CCO and Mn(H)CCO molecules on the basis of isotopic substitutions and density functional calculations of isotopic frequencies.

Acknowledgment. We greatly acknowledge financial support from NSFC (20203005 and 20125033) and the NKBRSF of China.

References and Notes

(1) Ryan, M. F.; Fiedler, A.; Schröder, D.; Schwarz, H. *J. Am. Chem. Soc.* **1995**, *117*, 2033.
(2) Sono, M.; Roach, M. P.; Coulter, E. D.; Dawson, J. H. *Chem. Rev.* **1996**, *96*, 2841.
(3) Wallar, B. J.; Lipscomb, J. D. *Chem. Rev.* **1996**, *96*, 2625.
(4) Solomon, E. I.; Brunold, T. C.; Davis, M. I.; Kemsley, J. N.; Lee, S. K.; Lehnert, N.; Neese, F.; Skulan, A. J.; Yang, Y. S.; Zhou, J. *Chem. Rev.* **2000**, *100*, 235.
(5) Miyake, H.; Chen, K.; Lange, S. J.; Que, L., Jr. *Inorg. Chem.* **2001**, *40*, 3534.
(6) van Koppen, P. A. M.; Bowers, M. T.; Haynes, C. L.; Armentrout, P. B. *J. Am. Chem. Soc.* **1998**, *120*, 5704.
(7) Schroder, D.; Schwarz, H. *Angew. Chem., Int. Ed. Engl.* **1995**, *34*, 1973.
(8) Eller, K.; Schwarz, H. *Chem. Rev.* **1991**, *91*, 1121.
(9) Armentrout, P. B.; Beauchamp, J. L. *Acc. Chem. Res.* **1989**, *22*, 315.
(10) Carroll, J. J.; Haug, K. L.; Weisshaar, J. C.; Blomberg, M. R. A.; Siegbahn, P. E. M.; Svensson, M. *J. Phys. Chem.* **1995**, *99*, 13955.
(11) Carroll, J. J.; Weisshaar, J. C. *J. Phys. Chem.* **1996**, *100*, 12355.
(12) Blitz, M. A.; Mitchell, S. A.; Hackett, P. A. *J. Phys. Chem.* **1991**, *95*, 8719.
(13) Kafafi, Z. H.; Hauge, R. H.; Margrave, J. L. *J. Am. Chem. Soc.* **1985**, *107*, 7550.
(14) Kline, E. S.; Kafafi, Z. H.; Hauge, R. H.; Margrave, J. L. *J. Am. Chem. Soc.* **1985**, *107*, 7559.
(15) Lee, Y. K.; Manceron, L.; Papai, I. *J. Phys. Chem. A* **1997**, *101*, 9650.
(16) Huang, Z. G.; Zeng, A. H.; Dong, J.; Zhou, M. F. *J. Phys. Chem. A* **2003**, *107*, 2329.
(17) Miao, L.; Dong, J.; Yu, L.; Zhou, M. F.*J. Phys. Chem. A* **2003**, *107*, 1935.
(18) Zhou, M. F.; Zhang, L. N.; Shao, L. M.; Wang, W. N.; Fan, K. N.; Qin, Q. Z. *J. Phys. Chem. A* **2001**, *105*, 5801.
(19) Zhou, M. F.; Zhang, L. N.; Qin, Q. Z. *J. Phys. Chem. A* **2001**, *105*, 6407.
(20) Shao, L. M.; Zhang, L. N.; Chen, M. H.; Lu, H.; Zhou, M. F. *Chem. Phys. Lett.* **2001**, *343*, 178.
(21) Dong, J.; Miao, L.; Zhou, M. F. *Chem. Phys. Lett.* **2002**, *355*, 31.
(22) Chertihin, G. V.; Andrews, L. *J. Phys. Chem. A* **1997**, *101*, 8547.
(23) Chertihin, G. V.; Saffel, W.; Yustein, Y. T. Andrews, L.; Neurock, M.; Ricca, A.; Bauschlicher, C. W., Jr. *J. Phys. Chem.* **1996**, *100*, 5261.
(24) Chen, M. H.; Wang, X. F.; Zhang, L. N.; Yu, M.; Qin, Q. Z. *Chem. Phys.* **1999**, *242*, 81.
(25) Frisch, M. J.; Trucks, G. W.; Schlegel, H. B.; Scuseria, G. E.; Robb, M. A.; Cheeseman, J. R.; Zakrzewski, V. G.; Montgomery, J. A., Jr.; Stratmann, R. E.; Burant, J. C.; Dapprich, S.; Millam, J. M.; Daniels, A. D.; Kudin, K. N.; Strain, M. C.; Farkas, O.; Tomasi, J.; Barone, V.; Cossi, M.; Cammi, R.; Mennucci, B.; Pomelli, C.; Adamo, C.; Clifford, S.; Ochterski, J.; Petersson, G. A.; Ayala, P. Y.; Cui, Q.; Morokuma, K.; Malick, D. K.; Rabuck, A. D.; Raghavachari, K.; Foresman, J. B.; Cioslowski, J.; Ortiz, J. V.; Baboul, A. G.; Stefanov, B. B.; Liu, G.; Liashenko, A.; Piskorz, P.; Komaromi, I.; Gomperts, R.; Martin, R. L.; Fox, D. J.; Keith, T.; Al-Laham, M. A.; Peng, C. Y.; Nanayakkara, A.; Gonzalez, C.; Challacombe, M.; Gill, P. M. W.; Johnson, B.; Chen, W.; Wong, M. W.; Andres, J. L.; Gonzalez, C.; Head-Gordon, M.; Replogle, E. S.; Pople, J. A. *Gaussian 98*, Revision A.7; Gaussian, Inc.: Pittsburgh, PA, 1998.
(26) Becke, A. D. *J. Chem. Phys.* **1993**, *98*, 5648.
(27) Lee, C.; Yang, E.; Parr, R. G. *Phys. Rev. B* **1988**, *37*, 785.
(28) McLean, A. D.; Chandler, G. S. *J. Chem. Phys.* **1980**, *72*, 5639.
(29) Krishnan, R.; Binkley, J. S.; Seeger, R.; Pople, J. A. *J. Chem. Phys.* **1980**, *72*, 650.
(30) Moore, C. B.; Pimentel, G. C. *J. Chem. Phys.* **1963**, *38*, 2816.
(31) Milligan, D. E.; Jacox, M. E.; Abouaf-Marquin, L. *J. Chem. Phys.* **1967**, *46*, 4562. Jacox, M. E. *Chem. Phys.* **1975**, *7*, 424.
(32) Milligan, D. E.; Jacox, M. E. *J. Chem. Phys.* **1963**, *38*, 2627.
(33) Smith, D. W.; Andrews, L. *J. Chem. Phys.* **1974**, *60*, 81.
(34) Pople, J. A.; Gordon, M. H.; Raghavachari, K. *J. Chem. Phys.* **1987**, *87*, 5968.
(35) Bauschlicher, C. W., Jr.; Langhoff, S. R. *Spectrochim. Acta A* **1997**, *53*, 1205.